PROCEEDINGS, 49th Workshop on Geothermal Reservoir Engineering
Stanford University, Stanford, California, February 12-14, 2024
SGP-TR-227

Feasibility of Measuring the Strain Tensor at Geothermal Reservoir Temperatures

Clem Laffaille, Josh Parris, Scott DeWolf, Leonid Germanovich, Lawrence C. Murdoch
Clemson University, 342 Computer Court, Anderson, CS, 29625
lmurdoc@clemson.edu

Keywords: EGS, strainmeter, strain, deformation, geothermal reservoir, FORGE

ABSTRACT

Monitoring and interpreting deformation from hydraulic fracturing or heat recovery promises to generate insights that can improve performance of enhanced geothermal systems (EGS). Borehole tensor strainmeters have been used to characterize in-situ deformation, but current strainmeter technology is unable to function at temperatures typical of geothermal reservoirs. The objective of this work is to evaluate the feasibility of measuring the strain tensor at high temperatures to meet the needs of applications at EGS sites. The approach has been to conduct simulations to evaluate the expected strain signals, and then design, build, and test a strainmeter that can measure these signals. A design for a high-temperature split-sleeve tensor strainmeter using optical fiber sensors embedded in a composite material was developed with the intent that it would be deployed behind casing during well completion. A prototype strainmeter was attached to a pipe simulating a casing and heated in an oven from 200ºC to 300ºC for nearly 6 months (178 days). Bending strain was created by periodically applying loads in two different directions normal to the end of the pipe. The instrument measured four components of strains in the range of ± 30 με with relative magnitudes that are consistent with strains predicted using a numerical simulation of the applied loads at temperatures below 250ºC. The instrument responded to applied load at temperatures in the 250ºC to 300ºC range, but the magnitude of the response decreased with temperature.

1. INTRODUCTION

Enhanced Geothermal Systems (EGS) rely on well stimulations methods to increase the rate of energy recovery (Held et al. 2014). Both well stimulation and energy recovery cause deformation in the vicinity of the operational wells, and this in turn causes deformation in a much broader region enveloping the EGS reservoir. The deformation ranges from brief, rapid events characterized by micro-seismicity, to continuous, slow changes in the strain tensor (Murdoch et al. 2020). A variety of instruments and optical fiber sensors are available to measure micro-seismicity, and recent developments in optical fiber borehole strainmeters have made it feasible to measure the strain tensor with high precision (Murdoch et al. 2019, 2023). Measuring multiple components of the strain tensor has the potential to provide more information about a strain-causing event than measurements of uniaxial strain (Murdoch et al, 2023; Roudini et al. 2023).

Optical fiber tensor strainmeters use only optical components downhole (DeWolf et al. 2015), so they avoid potential problems with downhole electronics. However, current optical fiber borehole strainmeter technology uses optical components that are rated for ambient temperatures at the ground surface (<80ºC), so it is poorly suited to downhole applications in geothermal reservoirs where temperatures can be greater than 200ºC. For example, the temperature at the bottom of the 16(A)78-32 well at Utah FORGE is 225ºC (EGI, 2018). This is far hotter than the rating of components used in current optical fiber borehole strainmeters, but there are alternative components with higher temperature ratings that could be used to extend the operational temperature range.

We are evaluating the feasibility of measuring multiple components of the strain tensor in a borehole at geothermal temperatures. This requires an instrument that can perform at reservoir temperatures and that can be integrated into the completion process used for geothermal wells. We have completed a preliminary evaluation of a prototype strainmeter and the objective of this paper is to describe the instrument and the results of the evaluation.

2. HIGH TEMPERATURE STRAINMETER

We developed a tensor strainmeter design that can be deployed on the outside of casing during well completion. It uses a tubular geometry that is split axially along one side (Figure 1). This split-sleeve design is opened and placed around a casing and then fasteners can be used to join the sleeve at the split and apply tension. It should be feasible to deploy strain sensors around nearly the entire circumference, and this would facilitate measuring the strain tensor normal to, and parallel to the axis of the casing. Optical fiber cable is routinely run in the annulus behind casing, and the split-sleeve strainmeter would be integrated into this existing system.

2.1 Sensors

Optical fiber strain sensors are embedded in the sleeve during construction of the instrument. A variety of optical fiber sensors are available to measure strain and the split-sleeve design can accommodate all of them. We used Fiber Bragg Gratings (FBGs) in polyimide-coated single mode fiber for testing in the laboratory because this system can measure strain relative to an arbitrary baseline even if the interrogator is temporarily disconnected. This makes it ideal for long-term applications in the laboratory. Interferometer-based sensors (DeWolf et al. 2015; Murdoch et al. 2020) can be used in the field where high-resolution strain measurements are required. Optical fiber designed to be interrogated by phase-sensitive optical time domain reflectometry (OTDR) methods of distributed acousting sensing (DAS) can also be used in the split-sleeve design.

2.2 Clamping

Sensors in the strainmeter should be put into tension prior to deployment. This facilitates measuring both expansion and contraction relative to an initial, tensioned state. This can be accommodated by putting the sleeve or shell in tension when it is clamped to the casing. One approach is to attach tensioning fixtures to the edge of the sleeve and draw the fixtures together with a bolt (Figure 1). A similar approach can be implemented by attaching straps to a shell and tensioning the straps during deployment.

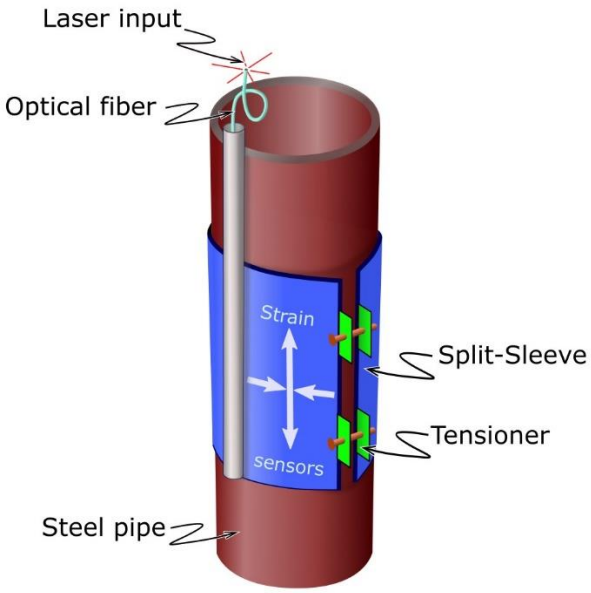

Figure 1. Design of the split-sleeve strainmeter wrapped around a steel pipe and clamped with tensioners. The split-sleeve strainmeter contains optical fiber sensors that measure multiple components of strain.

2.3 Split-sleeve

The split-sleeve was fabricated from a composite material that consists of E-glass fiber cloth embedded in Duralco 4461IP (Cotronics) epoxy resin. The fiberglass cloth was saturated with resin and applied to a male mold using a wet layup technique. The optical fiber was applied in a sigmoidal pattern with the first three FBGs strain sensors on the fiber (S1, S2, and S3) oriented axially and separated by 120º around the circumference of the sleeve. Sensor S4 was oriented circumferentially near S2. A stainless steel tube was bonded to the sleeve and used to protect the optical fiber between the sleeve and the interrogator (Figure 1). Additional layers of fiberglass cloth were applied over the optical fiber so the sensors and stainless steel tube were embedded between laminates in the final sleeve. Threaded fixtures were created from a forged carbon composite (Feraboli et al., 2010) and bonded on either side of an axial slit in the sleeve. These fixtures were used to tighten the sleeve onto a casing during operation. The resin was cured at room temperature for 24 hours and then heat-treated for 1 hour at 120ºC and 1 hour at 175ºC before use. The heat treating process strengthens the resin and is recommended by the epoxy resin manufacturer. Additional information about fabrication is in Laffaille (2024).

The Duralco 4461IP resin has the lowest temperature rating of the components. It is recommended for temperatures up to 260ºC, which is approximately the glass transition temperature. E-glass and carbon fiber are durable to temperatures of 1000ºC or greater. The coefficient of linear thermal expansion (CTE) of Duralco 4461IP resin is 54×10^{-6}/ºC, whereas the CTE of E-glass is much less, approximately 5×10^{-6}/ºC, and it is even less for carbon fiber, approximately 2×10^{-6}/ºC.

Strain measurements were made with a FiSens FBG X150 interrogator (808-865 nm wavelength range with 0.1 με precision; Micronor.com) using an array of four FBGs on Fibercore SM800, a single mode optical fiber coated with polyimide.

3. LABORATORY TESTING

The split-sleeve strainmeter was first tested in the laboratory for basic functionality properties and then a more comprehensive test was conducted to evaluate performance during heating and loading. An apparatus for heating and applying a load to a casing was developed, and then the split-sleeve strainmeter was attached to a casing in the apparatus and used to measure the response to applied loads at different temperatures over six months. The strain responses obtained over the first two months were then interpreted using simulations.

3.1 Apparatus

The experiments were conducted using an apparatus based around a cylindrical oven constructed using a 3-m-long 310 Watt BriskHeat heating cable wrapped around a 10-cm-diameter and 1.2-m long piece of sheet metal, which formed the inner wall of the oven. The duct and heater were wrapped with fiberglass insulation, and the assembly was enclosed in a 25-cm-diameter duct that was capped and sealed (Figure 2). A PID controller was tuned so temperature fluctuations in the oven were less than 5ºC.

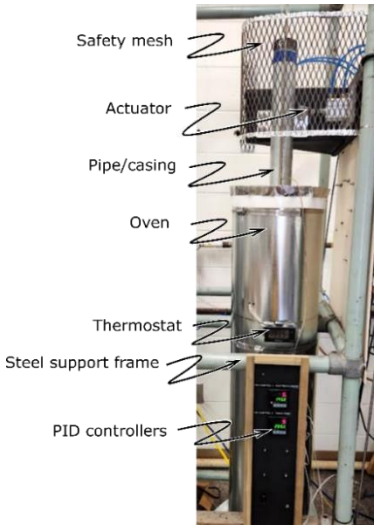

Figure 2. Oven with the split-sleeve strainmeter installed inside. Actuators load the upper end of the pipe/casing while the temperature in the oven is regulated by PID controllers.

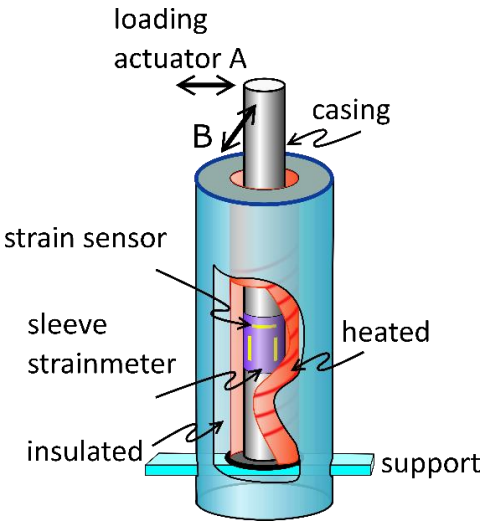

Figure 3. Schematic of experimental apparatus. The strainmeter (purple) is clamped on a steel pipe representing a casing and put in a heated oven. Actuators A and B load the pipe in two directions. Actuator A is parallel to the support of the casing.

A 1.5 m-long, 2-inch nominal steel pipe was mounted vertically inside the oven, and it served as a surrogate for well casing. The pipe/casing was threaded into a flange that was bolted to two, parallel 2.5-cm-wide box tubes. The box tubes are 90 cm long and bolted to a steel frame approximately 30 cm above the floor. The oven was mounted to the steel frame. The flange holding the pipe was wrapped in insulation, enclosed in sheet metal and sealed to form the bottom of the apparatus. The pipe extends through a seal in the oven and protrudes 30 cm above the top of the oven (Figure 2 and 3). This configuration has the pipe/casing fixed at the bottom and free at the top, and it is enclosed in the oven from its base to a height of 1.2 m. The pipe/casing is intended to function as a vertical cantilever with a fixed base. However, the threaded joint between the pipe and the flange may be more compliant than a welded joint. Moreover, flexing of the 2.5-cm-wide box tubing probably caused the base to be more compliant when the pipe is loaded perpendicular to tubing than when it is loaded parallel to the tubing. These factors may cause the base to depart from a perfectly rigid structure.

The pipe/casing was loaded with forces applied transverse to its axis. This was accomplished using two air cylinders configured as linear actuators. They are placed at 90° from each other and can push the pipe/casing either parallel to, or perpendicular to the underlying box tubing (Figure 2. Oven with the split-sleeve strainmeter installed inside. Actuators load the upper end of the pipe/casing while the temperature in the oven is regulated by PID controllers. and 3). The actuators are controlled by two solenoid valves and timers, which determine the duration and frequency of loading for each actuator.

A V-shaped fixture is attached to the end of the actuator in order to center the pipe when the actuator is extended. The force and range of the actuators were adjusted to apply sufficient pressure to the actuator, so it extended fully. This created a repeatable displacement condition for each cycle.

The actuator parallel to the box tubing was labeled Actuator A, and Actuator B was normal to it (Figure 3). The displacement at actuator A was 5 mm and it was 4 mm at actuator B. More information is in Laffaille (2024)

3.2 Thermal Expansion

A set of tests was conducted by heating the split-sleeve strainmeter while monitoring the strain to evaluate the effective coefficient of thermal expansion. One test involved heating the strainmeter alone. The other test involved attaching the strainmeter to a steel pipe and tightening the clamping mechanism to put the strainmeter in tension.

The strain increased as roughly a linear function of temperature when the strainmeter was attached to the pipe. The slope, and thus the apparent CTE ranges from 13 με/°C to 15 με/°C, and the mean is 14.5° με/°C (Figure 4b). The CTE of carbon steel ranges from 11 to 13 με/ºC (Cverna, 2002). The apparent CTE of the strainmeter alone during heating is similar to that of the strainmeter attached to the pipe, but the apparent CTE of the strainmeter decreases to less than 10 με/ºC at temperatures above 180ºC (Figure 4a).

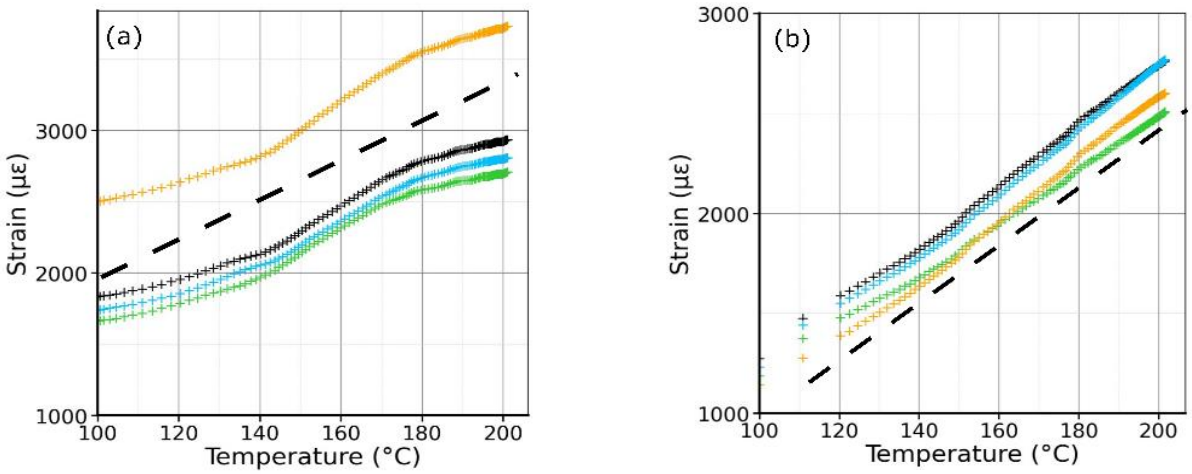

Figure 4. Strains function of temperature during heating from 100°C to 200°C. (a) Split-sleeve strainmeter alone. (b) Split-sleeve strainmeter on steel pipe. Dashed line indicates apparent CTE of 14 x 10-6 1/°C.

Results of the CTE tests indicate that the strainmeter expands approximately the same as a steel pipe or carbon steel casing during heating, and it may tighten on the pipe slightly when heated above 180ºC. This suggests that the coupling of the strainmeter to the casing is nearly unaffected by heating.

3.3 Durability test

The objective of this experiment is to characterize the ability of the strainmeter to measure strains over extended duration at geothermal reservoir temperatures.

3.3.1 Experiment design

The experiment was conducted by operating the oven at 200ºC for one month and then stepping up the temperature in increments of 20 to 30ºC, ultimately reaching 300ºC after six months (Figure 5a). The actuators were activated periodically throughout the test. Each actuator operated with a period of 20 sec (10 seconds when the actuator was extended and 10 seconds when it was retracted) for a total of 3 minutes (nine periods). Actuator A was activated for a 3-minute-long loading cycle, and then actuator B was activated for a 3-minute cycle and then they were both shut off for 54 minutes. This hour-long sequence was repeated every hour for the duration of the test. This generated step-like strain time series, with nine steps up and nine steps down at each sensor (Figure 6).

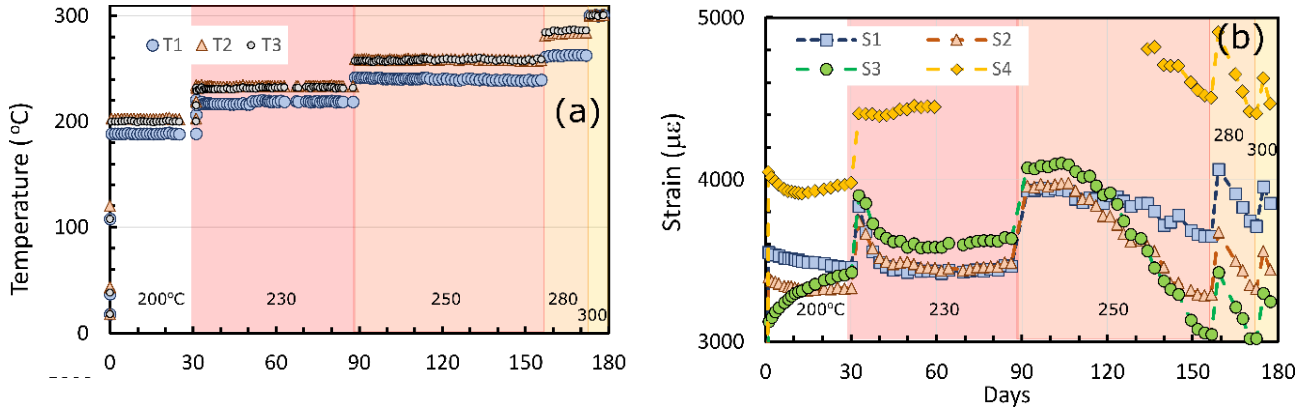

Figure 5. (a) Temperature as function of time in oven during the experiment. (b) Strains relative to ambient temperature measured at different sensors in split-sleeve strainmeter.

The strain data were analyzed by finding each loading cycle using a convolution function (Arfken et al., 2013) and then measuring the average strain value when an actuator was extended and subtracting the strain measured during the following interval when the actuator was retracted. The mean and standard deviation of the nine values for each loading cycle were then calculated every hour to give the strain response to load for each of the four FBGs and the two applied loads from actuator A and B. These values were then averaged over various longer intervals for evaluation and plotting.

Table 1. Strain magnitudes in response to load from experimental data for the first 20 days and from simulations. Baseline simulation considers uniform material, Scenario 1 considers a compliant junction between pipe and flange, Scenario 2 considers a compliant junction and a small component of displacement in -y direction during Load A. std dev= standard deviation, CoV = coefficient of variation, R.E.=relative error of simulations and data. Shaded cells are where |R.E.| > 0.2.

Data				Simulations					
FBG+Load	mean	std dev	CoV	Baseline	R.E	Scenario 1	R.E.	Scenario 2	R.E.
S1A	-6.2	1.3	-0.21	-43	-5.90	-12	-0.93	-6.8	-0.09
S1B	-13.6	1.4	-0.10	-21	-0.54	-11	0.19	-11	0.19
S2A	23.4	0.3	0.01	86	2.67	24	0.02	24.6	0.05
S2B	1.6	0.1	0.06	1E-03	-1.00	1E-04	-1.00		-1.00
S3A	-21.2	3.6	-0.17	-43	-1.03	-12	0.43	-17	0.20
S3B	11.6	2.0	0.18	21	0.81	11	-0.05	11	-0.05
S4A	-7.9	0.8	-0.10	-26	-2.30	-7.5	0.05	-7.4	0.06
S4B	-1.2	0.2	-0.13	-0.1	0.92	0	1.00		1.00

The noise in the signal was characterized as the standard deviation of 20 seconds of data before the load was applied. The signal to noise ratio was determined as the ratio of the maximum average strain amplitude during a cycle to the noise calculated before the load was applied.

3.3.2 Results

The axial strain increased abruptly by 3200 to 3600 με and the circumferential strain increased by 4200 με as a result of heating from ambient (20°C) to 200°C (Figure 5b). This is consistent with expansion due to heating. The axial strains increased by several 100 με each

time the temperature was increased, and then they gradually decreased and returned to roughly the strain value at 200°C. The circumferential strain increased during heating from 200 to 230°C, but it remained steady for the next few weeks. A problem with the data acquisition system prevented data from S4 from being saved from day 60 to 130 (Figure 5).

The strain responded to the applied loads from actuators A and B as a step-like time series (Figure 6) and the average magnitude of the steps was approximately ± 30 με over the duration of the test (Figure 7). Positive strain is tension, negative is compression. During the 200°C and 230°C heating periods, the amplitudes of the strain steps varied slightly with a coefficient of variation generally less than 0.3 for the first 20 days of the experiment (**Error! Reference source not found.**).

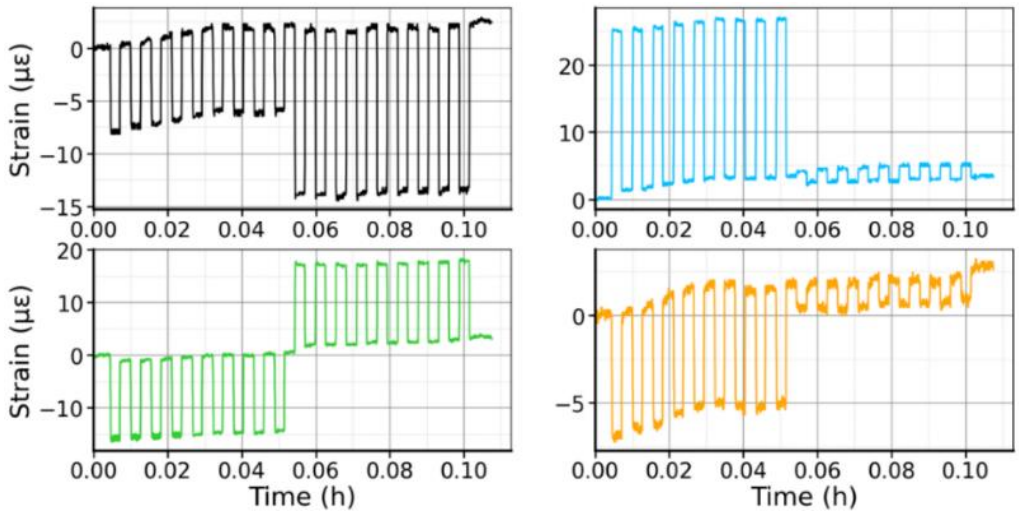

Figure 6. Baseline loading test where two loads were applied nine times resulting in strain changes. Measured data for each FBG sensor is represented: S1 (black), S2 (blue), S3 (green) and S4 (orange).

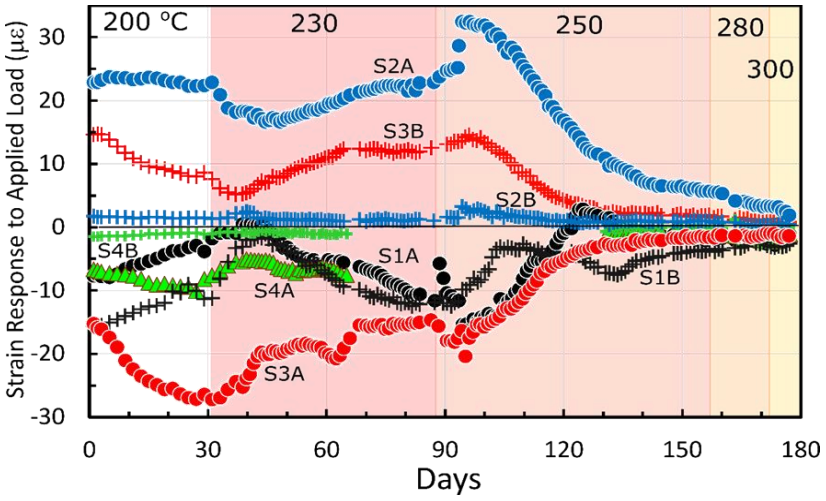

Figure 7. Average strains measured in response to periodic applied loads A and B at sensors S1, S2, S3, and S4 in split-sleeve strainmeter during the experiment.

The strain response to applied loads changed when the temperature was increased from 230 to 250°C. The strain response increased slightly when the temperature was first increased, but then it gradually decreased as roughly a negative exponential throughout the duration of the experiment (Figure 7. Average strains measured in response to periodic applied loads A and B at sensors S1, S2, S3, and S4 in split-sleeve strainmeter during the experiment.). The strain responses decreased to approximately ± 5 με at the end of the 250°C heating interval. The relative magnitudes of the tensile responses remained consistent throughout this period, but they changed for the compressive responses. The strain responses decreased further when the temperature was increased and the responses were ± 3 με during the 300°C heating interval. The experiment was terminated on day 179 after heating for 1 week at 300°C because the strain response was zero.

The signal to noise ratio was calculated every 20 days by using the amplitude of the strain response to load (Figure 7) as the signal and the standard deviation of the strain prior to the applied load as a measure of the noise. The SNR is greater than 10 for the first 130 days of the experiment, except for a brief period when S1A decreased below 10 around day 30.

4. SIMULATIONS

Simulations of the experiment were conducted to evaluate and interpret the strain response to loads. It was difficult to independently measure strain in the casing during the experiments, so we used simulations to estimate the expected strain, which was then compared to the experimental data.

The simulations included the pipe/casing as well as a flange and box tubing used for mounting the pipe/casing (Figure 8). Linear elastic deformation was assumed with traction free boundary conditions everywhere except at the ends of the box tubing, which were assumed to have zero displacement. Another boundary condition was a specified transverse displacement at the end of the pipe/casing to represent Loads A (u_x =-5mm) and B (u_y=4mm). All the components were made from carbon steel, so Young's Modulus was assumed to be E = 200 GPa and Poisson's ratio was ν = 0.3 (Gandy, 2007).

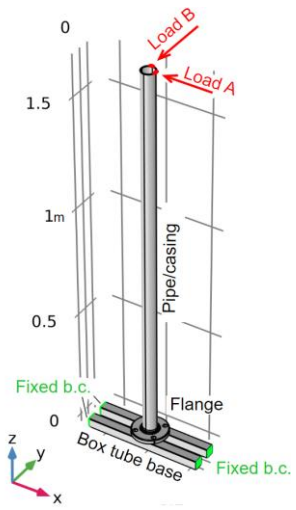

Figure 8. Geometry and boundary conditions used in the simulations.

Three scenarios were considered to evaluate different effects: a Baseline scenario assumes the material properties are uniform and the displacements for Loads A and B are uniaxial. Scenario 1 considers a junction between the pipe and flange that is compliant. This could be a result of the material removed at the threads or slight loosening at the threaded junction. The compliant junction was represented using E = 0.7 GPa at the junction. Scenario 2 was developed to explain the difference between the S1A and S3A strains. This scenario includes u_y = 2 mm Load A. More details about the simulations are in Laffaille (2024).

4.1 Simulation Results

The baseline scenario was evaluated using a transient analysis that considered two cycles of A loading followed by two cycles of B loading. The specified displacement was applied for 10 seconds and released for 10 seconds, following the experimental conditions. The predicted strains at the sensor locations are periodic square waves with magnitudes that vary with the location of the measurement and the load. The largest strain response is a magnitude of more than 80 με and it occurs at S2 during loading A, and the strains are equal or less than -40 με at S1 and S3 during loading A.

The magnitudes of the strain responses in the simulations relative to each other are similar to the experimental data, but the simulated magnitudes are roughly three times larger than those in the experiments (Table 1). One explanation for this is the joint between the pipe and the flange is more compliant than assumed in the baseline model. Scenario 2 included a more compliant joint between the pipe and the flange to evaluate this scenario. The data for Scenario 2 in Table 1 were obtained using E = 0.7 GPa for the effective Young's modulus of the joint. This change reduces the magnitudes of the strain steps by approximately a factor of three because it reduces the curvature of the pipe (Figure 9).

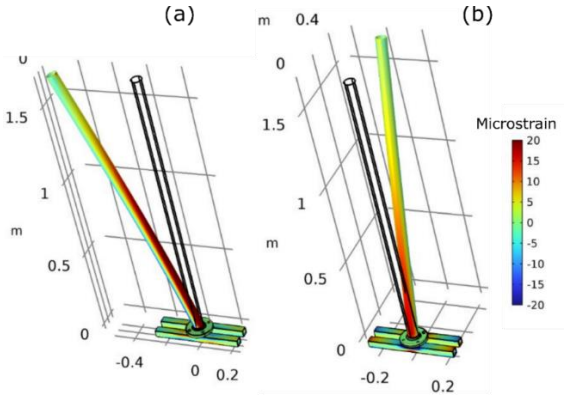

Figure 9. Perspective view of pipe/casing, flange and box tubing with vertical strain as color during (a) Load A and (b) Load B. Apparatus is displaced with exaggeration of 100x. Color is vertical strain.

The relative errors from Scenario 1 are less than from the Baseline scenario, but the errors in four of the channels are greater than 0.2 (shaded in Table 1), so additional factors were considered to account for this error. The magnitudes of S2B and S4B in the data (1.6 and -1.2 με) are smaller than in the other datasets, and the simulation predicts that these values should be zero. This causes a high relative error, but the absolute error is small, so it appears that the simulation predicts these values with sufficient accuracy.

The magnitudes of S1A and S3A are predicted to be equal in the Baseline and Scenario 1 because sensors S1 and S3 are symmetric about the line of Load A. However, the magnitude of S1A observed in the data (6.2 με) is greater than, and that of S3A (21 με) is less than the predicted value of 12 με. This suggests that a factor that breaks symmetry is responsible for the error. One possibility is that S1 and S3 are not symmetric about the line of Load A (x-axis). This could occur if the strainmeter was unexpectedly rotated, or if the locations of the strain sensors where shifted during fabrication of the strainmeter. These factors would cause S1B results to differ from S3B, but the data indicate that these values are essentially the same (within 1 standard deviation).

Another possibility is that there is a small displacement in the *y*-direction during Load A. This could occur, for example, if the V-shaped fixture at end of the actuator was displaced slightly from the center line so one side of the V contacted the pipe before the other side. To evaluate this possibility a displacement of -0.002 m in the y-direction was included in Loading A, along with the displacement of -0.005 m that was used in the other scenarios. This decreases the strain at S1A and increases it at S3A. The relative error of the resulting strains (Table 1) are all less than 0.2 (ignoring the R.E. at S2B and S4B as justified above).

5. DISCUSSION

The split-sleeve strainmeter was able to measure strain response to load throughout the 178-day-long experiment where temperatures ranged from 200 to 300ºC. The magnitudes of the responses in the 200ºC and 230ºC ranges are consistent with magnitudes expected from a bending elastic tube, based on finite element simulations. The slow decrease in magnitude once temperatures reach 250ºC appears to result from a softening of the resin used to create the sleeve. Softening would decrease the strain transfer from the casing to the fiber, which would explain the reduction in response.

The resin is rated to 260ºC by the manufacturer, but it likely softens at a higher temperature. The data suggest that the strainmeter behavior was stable in the range of 200 to 230ºC and the behavior changed as the temperature increased to 250ºC. Even though the magnitude of the strain response decreased with time and temperature, the strainmeter continued to respond to strain for 7 days at 300ºC. This indicates that the strainmeter could provide meaningful data on the timing of strain events, but the apparent strain magnitude would be less than the actual magnitude.

These results indicate that the strainmeter configuration tested could function for an extended period at temperatures anticipated in geothermal reservoir at Utah FORGE (225ºC). We are currently evaluating an alternative resin that is rated to 315ºC by the manufacturer and we anticipate that it would not soften at temperature greater than those cited above.

The strainmeter ultimately stopped providing data after 7 days at 300ºC, and we expect this was because the optical fiber broke. We used optical fiber with a polyimide coating that was rated for service to 300°C. When the strength of the polyimide coating is degraded, stresses supported by the coating will be transferred to the cladding and core, breaking the fiber. This effect appears to define the current upper temperature limit of operation.

As it is difficult to obtain an independent measurement strain in the pipe/casing during heating, we used a finite element simulation to infer that the joint between the pipe/casing and a mounting flange was flexing to account for the measured strains being less than the simulated baseline. Strain sensors on the pipe/casing would have provided a direct comparison to the strainmeter data. This is important because an alternative explanation for the difference between the Baseline simulation and the experimental data (Table 1) is that there is incomplete strain transfer from the pipe to the strain sensors. We are currently developing an experimental apparatus that will enable strains to be measured on the pipe/casing during heating so that future experiments can characterize strain transfer directly.

6. CONCLUSION

The experiment described above demonstrates that it is feasible to measure multiple components of strain with a composite, split-sleeve strainmeter (Figure 1) on a steel tube at temperatures similar to a geothermal reservoir (Figure 5) for extended periods lasting many months (Figure 7). We are optimistic that this work will lead to capabilities to measure multiple components of the strain tensor and seismicity in geothermal reservoirs.

7. ACKNOWLEDGEMENT

We appreciate the funding for this work provided by U.S DOE under grant DE-EE0007080 3-2514 “Enhanced Geothermal System Concept Testing and Development at the Milford City, Utah FORGE Site”. We thank Jess McDaniel and Jack Horvath for their help with the lab experiments.

REFERENCES

Arfken, G. B., Weber, H. J., & Harris, F. E.: Integral Transforms, Mathematical Methods for Physicists, (2013), 963–1046.

Dewolf, S., Wyatt, F. K., Zumberge, M. A., & Hatfield, W.: Improved vertical optical fiber borehole strainmeter design for measuring Earth strain, Review of Scientific Instruments, 86, (2015), 114502-114502-12.

EGI at the University of Utah.: Phase 2B Final Topical report, Frontier Observatory for Research in Geothermal Energy, (2018), 5-9.

Feraboli, P., Gasco, F., Wade, B., Maier, S., Kwan, R., Masini, A., Deoto, L., & Reggiani, M.: Technology for the suspension arms of the Sesto Elemento, Lamborghini Forged Composite", (2011), 7-8.

Gandy, D.: Chapter 5: Properties, Carbon Steel Handbook, (2007), 5-1-5-3.

Held, S., Genter, A., Kohl, T., Kölbel, T., Sausse, J., & Schoenball, M.: Economic evaluation of geothermal reservoir performance through modeling the complexity of the operating EGS in Soultz-sous-Forêts, Geothermics, 51, (2014), 270–280.

Laffaille C.: Using Strainmeters to Characterize Enhanced Geothermal Systems, Master of Science Thesis, Clemson University, Clemson, SC (2024).

Moore, J., Mclennan, J., Allis, R., Pankow, K., Simmons, S., Podgorney, R., Wannamaker, P., Bartley, J., Jones, C., & Rickard, W.: The Utah Frontier Observatory for Research in Geothermal Energy (FORGE): An International Laboratory for Enhanced Geothermal System Technology Development, Proceedings, (2019), 5-10.

Murdoch, L.C, DeWolf S., Germanovich L., Hanna A., Moak R. and Moysey S.: Characterizing and Interpreting the In Situ Strain Tensor During CO2 Injection. Final Report for DOE Project DE-FE 0023313, (2019). 252 p.

Murdoch, L. C., Germanovich, L. N., DeWolf, S. J., Moysey, S. M. J., Hanna, A. C., Kim, S., & Duncan, R. G.: Feasibility of using in situ deformation to monitor CO2 storage, International Journal of Greenhouse Gas Control, 93, (2020).

Murdoch, L. C., DeWolf S., Hua L., Germanovich L., Xiao H., Zhu X., Yongji W., Guo J., Moak R., Blais R., Roudini S., Costantino O., Plunkett G., Smith-Jones A.: Robust In-Situ Strain Measurements to Monitor CO2 Storage. Final Report for US DOE Project De-FE0028292, (2023), 692 p.

Murdoch, L. C., DeWolf, S., Germanovich, L. N., Moysey, S., Hanna, A., Roudini, S., & Moak, R.: Using the shallow strain tensor to characterize deep geologic reservoirs. *Water Resources Research*, 59, (2023).

Roudini S., Murdoch L., Shojaei M., DeWolf S.: Proxy-based Bayesian inversion of strain tensor data measured during well tests. Geomechanics for Energy and the Environment, 36, (2023).